GEOPHYSICS, VOL. 71, NO. 2 (MARCH-APRIL 2006); P. W1–W14, 8 FIGS.
10.1190/1.2187814

Tutorial

Amplitude, Fresnel zone, and NMO velocity for PP and SS normal-incidence reflections

Einar Iversen[1]

ABSTRACT

Inspired by recent ray-theoretical developments, the theory of normal-incidence rays is generalized to accommodate P- and S-waves in layered isotropic and anisotropic media. The calculation of the three main factors contributing to the two-way amplitude — i.e., geometric spreading, phase shift from caustics, and accumulated reflection/transmission coefficients — is formulated as a recursive process in the upward direction of the normal-incidence rays. This step-by-step approach makes it possible to implement zero-offset amplitude modeling as an efficient one-way wavefront construction process. For the purpose of upward dynamic ray tracing, the one-way eigensolution matrix is introduced, having as minors the paraxial ray-tracing matrices for the wavefronts of two hypothetical waves, referred to by Hubral as the normal-incidence point (NIP) wave and the normal wave. Dynamic ray tracing expressed in terms of the one-way eigensolution matrix has two advantages: The formulas for geometric spreading, phase shift from caustics, and Fresnel zone matrix become particularly simple, and the amplitude and Fresnel zone matrix can be calculated without explicit knowledge of the interface curvatures at the point of normal-incidence reflection.

INTRODUCTION

For thirty years, the theory of normal-incidence rays has garnered great attention and enthusiasm among researchers in the field of seismic exploration. The period around 1980 was especially creative for the development of ray theory in general and for the theory of normal-incidence rays in particular. Hubral and Krey (1980) give an excellent explanation of the normal-incidence ray concept and its role in seismic modeling, processing, and velocity estimation. It must be noted, however, that the normal-incidence ray was introduced with the assumptions of isotropic layers and P-wave mode along the entire path. Such limitations do not seem to harmonize with the current focus on anisotropy and S-waves within seismic exploration. Therefore, the principal objective of this paper is to present an updated theory for normal-incidence rays that takes into account propagation of P- and S-waves in isotropic and anisotropic structures.

A normal-incidence ray is, by definition, subjected to a normal-incidence reflection at some point located on the ray. For this NIP, I use the notation M, and the surface on which M is situated is the NIP interface (see Figure 1a). The original understanding of a normal-incidence reflection, based on the assumption of isotropy, is that the ray is normal to the interface at point M. For anisotropic conditions, this is not necessarily the case, but to avoid complicating the terminology, I prefer to use the term normal-incidence rays even for anisotropic media. Such rays are understood to carry a normal-incidence property — namely, the slowness vector of incidence is normal to the NIP interface. Other characteristics of the normal-incidence ray are that the source point S and the receiver point R coincide (at point X in Figure 1a) and that the one-way rays referred to as the source ray ($S \rightarrow M$) and the receiver ray ($R \rightarrow M$) are identical. The upward and downward directions of the normal-incidence ray are understood, respectively, as the directions $M \rightarrow X$ and $X \rightarrow M$.

Normal-incidence rays have many applications. The most obvious of these is modeling synthetic seismograms for the zero-offset case. A zero-offset survey is a virtual seismic survey configuration where only one receiver point is attached to each source point and where the source and receiver occupy the same position. Other applications are mapping arrivals from the zero-offset time domain to the depth domain, calculating normal moveout (NMO) velocities and corresponding

Manuscript received by the Editor November 22, 2004; revised manuscript received May 20, 2005; published online March 9, 2006.
[1]NORSAR, P.O. Box 53, 2027 Kjeller, Norway. E-mail: einar.iversen@norsar.com.

approximations for traveltimes in the common midpoint (CMP) domain, and estimating Fresnel zones and Fresnel volumes.

The objective of any zero-offset modeling approach is to simulate a physical wave that is initiated as a point source at the coinciding source/receiver point and then is propagated downward to a certain interface, where it is reflected and propagated back to the source/receiver (Figure 2a). For simplicity, I refer to this physical wave as the reflected wave.

An important relation to the normal-incidence ray is provided by Hubral (1983). He shows that the wavefront curvatures of the reflected wave can be expressed as a sum of the wavefront curvatures of two hypothetical waves corresponding to upward (one-way) propagation along the normal-incidence ray. These one-way waves are (1) the normal wave (Figure 2b), with the initial condition that the curvature matrix of the wavefront at point M is equal to the interface curvature matrix, and (2) the NIP wave (Figure 2c), which is initialized as a point source at M. Hubral and Krey (1980) and Chernyak and Gritsenko (1979) have proved the so-called NIP-wave theorem, which states that knowledge of the second derivatives of the traveltime function for the NIP wave is sufficient for determinating a second-order approximation to the traveltime within the CMP domain (Appendix E). Ursin (1982) develops quadratic approximations to the traveltime (parabolic approximation) and the traveltime squared (hyperbolic approximation) valid for finite-offset rays in the vicinity of a reference normal-incidence ray. Gjøystdal et al. (1984) compare the two approximations for 3D models of different complexity. Iversen and Gjøystdal (1984) utilize the NIP-wave theorem in a tomographic-inversion process based on minimizing the misfit between observed and computed NMO velocities.

The kinematic attributes of the reflected wave, e.g., the traveltime $T(R, S)$, are obtained trivially by one-way tracing of the normal-incidence ray. On the other hand, the determination of dynamic attributes by a one-way process is far from trivial. This problem is addressed by Hubral et al. (1993),

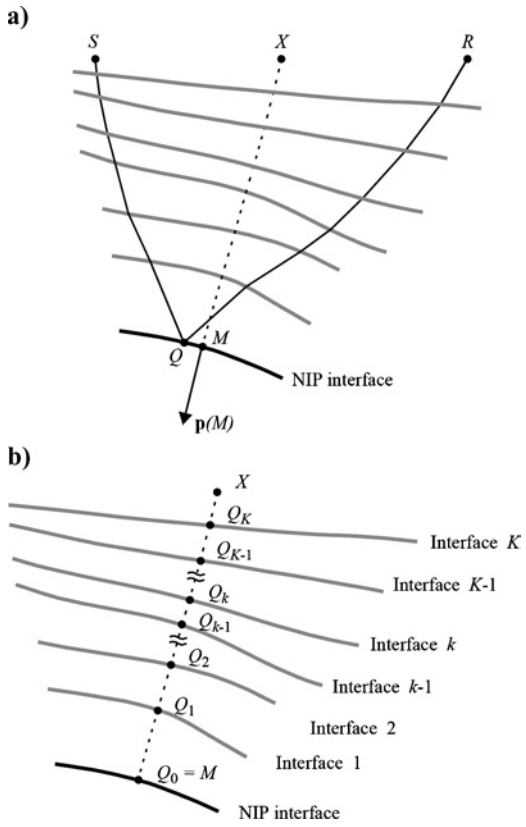

Figure 1. (a) Normal-incidence ray (dashed) with coinciding source/receiver at point X and normal-incidence point M. The slowness vector $\mathbf{p}(M)$ is normal to the NIP interface. Finite-offset ray (solid) is for source point S, receiver point R, common midpoint X, and reflection point Q. (b) Numbering of ray/interface intersection points in a recursive scheme for amplitude calculation in the upward direction along the normal-incidence ray.

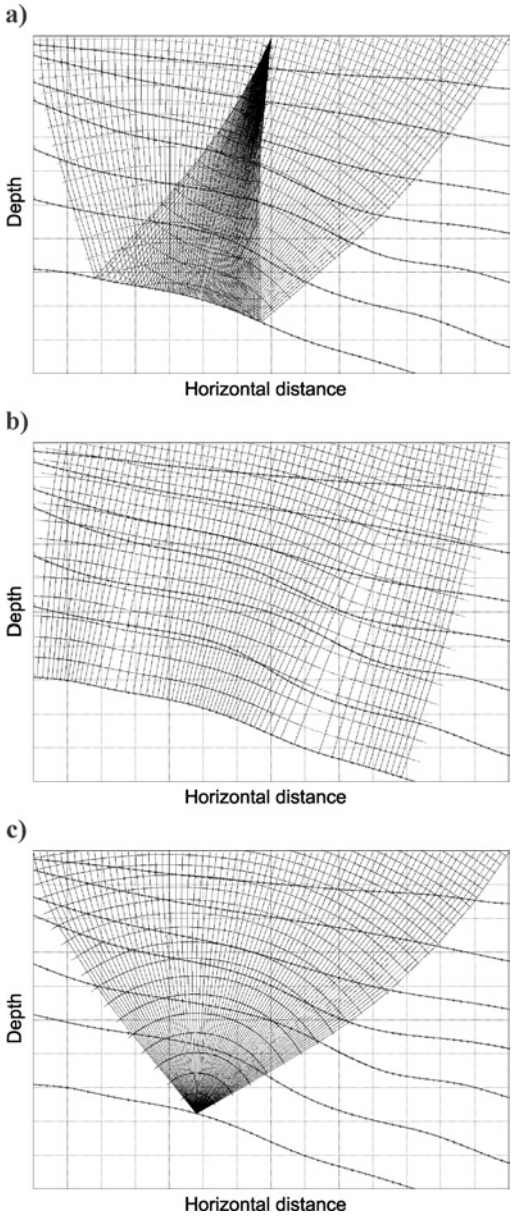

Figure 2. Rayfields corresponding to waves associated with normal-incidence rays. (a) The physical reflected wave. (b) The hypothetical normal wave. (c) The hypothetical NIP wave.

assuming the reflected wave to be a P-wave propagating in a 3D isotropic elastic medium. For a perfectly elastic medium, the amplitude of the reflected wave is influenced by three main propagation effects: the geometric spreading, the phase shift from caustics that affects the shape of the recorded signal, and the accumulated effect of reflection and transmission at interfaces. Hubral et al. (1993) focus on the estimation of the two former quantities by use of dynamic ray tracing (Červený, 1985) and surface-to-surface ray-propagator theory (Bortfeld, 1989). Assuming the complete normal-incidence ray to be known, they show that the geometric spreading and the phase shift from caustics can be obtained by dynamic ray tracing, either in the downward or upward direction. A particularly striking result is that a single downward integration of the dynamic ray-tracing system, with the initial condition of a point source, is sufficient to obtain both quantities.

In this paper I address aspects of the theory of normal-incidence rays that extend the generality considered by Hubral et al. (1993). The reflection at the normal-incidence point is allowed to be PP or SS, and the velocity model may consist of isotropic and anisotropic elastic layers. In the case of S-wave propagation in anisotropic layers, I consider elementary S-wave modes only (e.g., S1 or S2) that are completely decoupled (not exposed to singularities). An important objective has been to reformulate the equations for the two-way geometric spreading, the phase shift resulting from caustics, and the accumulated effect of reflection/transmission to make possible an efficient step-by-step calculation in the upward direction.

The presented aspects are based on five theoretical building blocks: (1) the theory of (standard) ray-propagator matrices (Červený, 1985), (2) the theory of surface-to-surface ray-propagator matrices (Bortfeld, 1989), (3) the theory expressing seismic attributes for the reflected wave in terms of the wavefront curvatures of the NIP wave and the normal wave (Hubral, 1983), (4) the theory expressing seismic attributes for the reflected wave in terms of surface-to-surface ray-propagator matrices (Hubral et al., 1983), and (5) the theory describing reciprocity of normalized reflection/transmission coefficients for isotropic and anisotropic media (Chapman, 1994; Červený, 2001).

The paper is organized in four sections describing the methodology, followed by a section including numerical examples. The first section presents formulas for one-way (upward) calculation of the reflected-wave amplitude of P and S types. The second section reviews the theories of standard ray-propagator matrices and surface-to-surface ray-propagator matrices. Based on these theories, I introduce in the third section the one-way eigensolution matrix for the normal-incidence ray. The fourth section describes the determination of various seismic attributes: relative geometric spreading, the Fresnel zone matrix, phase shift as a result of caustics, and NMO velocity related to the traveltime function of the CMP domain.

RAY AMPLITUDES

In the first of two subsections, I write the basic formulas describing the amplitudes of generally reflected and transmitted rays in a form applicable to models containing isotropic and anisotropic layers. The second subsection concentrates specifically on the computation of amplitudes along normal-incidence rays.

Finite-offset rays

For a ray with separated start and end points S and R, the high-frequency approximation to the displacement vector of a body wave is

$$\mathbf{u}(R,t) = \hat{\mathbf{U}}(R)F[t - T(R,S)]. \tag{1}$$

In equation 1, the time variable is denoted as t, and $T(R,S)$ is the traveltime along the ray. The scalar function F is a high-frequency, complex-valued signal consisting of the source wavelet (real part) and its Hilbert transform (imaginary part); $\hat{\mathbf{U}}$ denotes the vectorial ray-theory, complex-valued amplitude function. Equation 1 is valid for any coordinate system but is considered here for a local Cartesian system specified by three orthonormal basis vectors $\mathbf{f}^{(m)}$, $m = 1, 2, 3$. The basis $\mathbf{f}^{(m)}$ is defined differently for anisotropic and isotropic conditions. If the medium is anisotropic, $\mathbf{f}^{(m)} = \mathbf{g}^{(m)}$, where $\mathbf{g}^{(1)}$, $\mathbf{g}^{(2)}$, and $\mathbf{g}^{(3)}$ are the unit polarization vectors for, respectively, the S1-wave, the S2-wave, and the P-wave. We assume that vectors $\mathbf{g}^{(1)}$ and $\mathbf{g}^{(2)}$ can be determined uniquely as eigenvectors of the Christoffel matrix. If the medium is isotropic, a natural choice for $\mathbf{f}^{(m)}$ is the basis of the ray-centered coordinate system (Popov and Pšenčík, 1978), i.e., $\mathbf{f}^{(m)} = \mathbf{e}^{(m)}$ for $m = 1, 2, 3$. The vector $\mathbf{e}^{(3)}$ is tangent to the ray and parallel to the slowness vector in this case.

Formulas for components of the amplitude vector $\hat{\mathbf{U}}$ corresponding to a point source at S are given separately for isotropic and anisotropic structures (Červený, 2001, 458 and 510). Using the basis $\mathbf{f}^{(m)}$, the two formulations can be combined as

$$\hat{\mathbf{U}}^{(f)}(R) = \left[\frac{\rho(S)c(S)}{\rho(R)c(R)}\right]^{1/2} \times \frac{\exp[iT^c(R,S)]}{\mathcal{L}(R,S)}\hat{\boldsymbol{\mathcal{R}}}^C\hat{\boldsymbol{\mathcal{G}}}^{(f)}(S;\gamma_1,\gamma_2). \tag{2}$$

Here, c denotes the phase velocity of the wave under consideration at points S and R (P- or S-wave if the medium is isotropic; P-, S1-, or S2-wave if the medium is anisotropic) and ρ is the density. The quantities T^c and $\mathcal{L}$ denote, respectively, the total phase shift from caustics and the relative geometric spreading along the ray. The quantity $\hat{\boldsymbol{\mathcal{G}}}^{(f)}$ in equation 2 is the so-called 3×1 radiation matrix, having as arguments the ray parameters γ_1 and γ_2, e.g., two angles specifying the direction of the slowness vector at S, and $\hat{\boldsymbol{\mathcal{R}}}^C$ is the 3×3 matrix of accumulated normalized reflection/transmission (R/T) coefficients. The matrix $\hat{\boldsymbol{\mathcal{R}}}^C$ is given as a product of 3×3 matrices of normalized R/T coefficients, one such matrix for each interface encountered along the ray. For K ray/interface intersections in points $Q_1, Q_2, \ldots, Q_K$, we have

$$\hat{\boldsymbol{\mathcal{R}}}^C = \prod_{k=K}^{1}\hat{\boldsymbol{\mathcal{R}}}^T(Q_k) = \hat{\boldsymbol{\mathcal{R}}}^T(Q_K)\hat{\boldsymbol{\mathcal{R}}}^T(Q_{K-1})\ldots\hat{\boldsymbol{\mathcal{R}}}^T(Q_1). \tag{3}$$

The matrix of normalized R/T coefficients at a specific point Q_k is related to the matrix $\hat{\mathbf{R}}$ of (nonnormalized) R/T

coefficients by

$$\hat{\mathcal{R}}(Q_k) = \hat{\mathbf{R}}\left[\frac{\rho(\tilde{Q}_k)v(\tilde{Q}_k)\cos\psi(\tilde{Q}_k)}{\rho(Q_k)v(Q_k)\cos\psi(Q_k)}\right]^{1/2}. \quad (4)$$

Here, Q_k and $\tilde{Q}_k$ refer, respectively, to the sides of incidence and departure at point Q_k. The symbol ψ is used for the acute angle between the interface normal and the group velocity vector. The group velocity is the length of the group velocity vector, and is denoted as v. To calculate the R/T coefficients R_{ij} of matrix $\hat{\mathbf{R}}$, see the detailed description in Červený (2001).

An important property of the matrix $\hat{\mathcal{R}}$ is reciprocity, meaning that

$$\hat{\mathcal{R}}(\tilde{Q}_k) = \hat{\mathcal{R}}^T(Q_k). \quad (5)$$

Thus, the normalized matrix of R/T coefficients of a plane wave approaching point Q_k in the reverse direction of the ray ($R \rightarrow S$) is equal to the transpose of the corresponding matrix of the plane wave approaching Q_k in the forward direction ($S \rightarrow R$). The vectorial amplitude functions before and after reflection or transmission in a point Q_k are connected by the linear relation

$$\hat{\mathbf{U}}^{(f)}(\tilde{Q}_k) = \hat{\mathbf{R}}^T(Q_k)\hat{\mathbf{U}}^{(f)}(Q_k). \quad (6)$$

Equations 2–6 can be simplified considerably for specific wave types. For example, if a P-wave is to be simulated along the entire ray, the formula for the complex-valued amplitude has the scalar form

$$U_3^{(f)}(R) = \left[\frac{\rho(S)c(S)}{\rho(R)c(R)}\right]^{1/2} \times \frac{\exp[iT^c(R,S)]}{\mathcal{L}(R,S)}\mathcal{R}^C\mathcal{G}_3^{(f)}(S;\gamma_1,\gamma_2), \quad (7)$$

where the coefficient $\mathcal{R}^C$ is given by the product

$$\mathcal{R}^C = \prod_{k=1}^{K}\mathcal{R}(Q_k) = \mathcal{R}(Q_1)\boldsymbol{\mathcal{R}}(Q_{K-1})\ldots\mathcal{R}(Q_K). \quad (8)$$

A formula similar to equation 7 pertaining to isotropic layers is obtained by Ursin (1990).

Normal-incidence rays

Consider again the 3×3 matrices of normalized R/T coefficients in equations 4 and 5, but let Q_k be situated on a normal-incidence ray. The matrices $\hat{\mathbf{R}}(Q_k)$ and $\hat{\mathbf{R}}(\tilde{Q}_k)$ now correspond to propagation, respectively, in the upward and downward direction along the normal-incidence ray. I infer from equations 4 and 5 that

$$\hat{\mathbf{R}}^T(\tilde{Q}_k) = \hat{\mathbf{R}}(Q_k)\frac{\rho(\tilde{Q}_k)v(\tilde{Q}_k)\cos\psi(\tilde{Q}_k)}{\rho(Q_k)v(Q_k)\cos\psi(Q_k)}. \quad (9)$$

For the normal-incidence ray, the sequence of ray/interface intersection points $Q_k, k = 0, 1, \ldots, K$, corresponds to the upward direction along the ray, with Q_0 as the normal-incidence point (Figure 1b). Since the source and receiver coincide, we have $\rho(S) = \rho(R)$, and the symmetry of the source and receiver rays gives $c(S) = c(R)$. Based on equation 2 as well as on the reciprocal property of matrices of normalized R/T coefficients in equation 5, the vectorial amplitude function corresponding to two-way propagation, obtained solely by one-way calculations, is

$$\hat{\mathbf{U}}^{(f)}(R) = \frac{\exp[iT^c(R,S)]}{\mathcal{L}(R,S)}\prod_{k=1}^{K}\left[\frac{\rho(\tilde{Q}_k)v(\tilde{Q}_k)\cos\psi(\tilde{Q}_k)}{\rho(Q_k)v(Q_k)\cos\psi(Q_k)}\right] \times\prod_{k=K}^{1}\hat{\mathbf{R}}^T(Q_k)\hat{\mathbf{R}}^T(M)\prod_{k=1}^{K}\hat{\mathbf{R}}(Q_k)\hat{\boldsymbol{\mathcal{G}}}^{(f)}(S;\gamma_1,\gamma_2). \quad (10)$$

Equation 10 is well suited for a recursive calculation of the two-way amplitude function in the upward direction of the normal-incidence ray. One can rewrite the equation as

$$\hat{\mathbf{U}}^{(f)}(R) = \frac{\exp[iT^c(R,S)]}{\mathcal{L}(R,S)}\hat{\boldsymbol{\mathcal{R}}}^C(Q_K)\hat{\boldsymbol{\mathcal{G}}}^{(f)}(S;\gamma_1,\gamma_2), \quad (11)$$

where the 3×3 matrix $\hat{\boldsymbol{\mathcal{R}}}^C(Q_K)$ includes the accumulated normalized R/T coefficients corresponding to the two-way sequence of points $Q_K \rightarrow M \rightarrow Q_K$. A natural way to proceed during the calculation of $\hat{\boldsymbol{\mathcal{R}}}^C(Q_K)$ is to do the operation

$$\hat{\boldsymbol{\mathcal{R}}}^C(Q_k) = \frac{\rho(\tilde{Q}_k)v(\tilde{Q}_k)\cos\psi(\tilde{Q}_k)}{\rho(Q_k)v(Q_k)\cos\psi(Q_k)} \times\hat{\mathbf{R}}^T(Q_k)\hat{\boldsymbol{\mathcal{R}}}^C(Q_{k-1})\hat{\mathbf{R}}(Q_k) \quad (12)$$

successively for the values $k = 1, 2, \ldots, K$. The process is initialized for $k = 0$ by setting

$$\hat{\boldsymbol{\mathcal{R}}}^C(Q_0) = \hat{\mathbf{R}}^T(M). \quad (13)$$

If the wave mode is P along all ray segments, there will be only R/T coefficients of type PP. From equations 11–13, the two-way P-wave amplitude coefficient is then given by

$$U_3^{(f)}(R) = \frac{\exp[iT^c(R,S)]}{\mathcal{L}(R,S)}\mathcal{R}^C(Q_K)\boldsymbol{\mathcal{G}}_3^{(f)}(S;\gamma_1,\gamma_2). \quad (14)$$

Here, the scalar $\mathcal{R}^C(Q_K)$ can be obtained recursively for $k = 1, 2, \ldots, K$ by the formula

$$\mathcal{R}^C(Q_k) = \frac{\rho(\tilde{Q}_k)v(\tilde{Q}_k)\cos\psi(\tilde{Q}_k)}{\rho(Q_k)v(Q_k)\cos\psi(Q_k)}[R_{33}(Q_k)]^2\mathcal{R}^C(Q_{k-1}), \quad (15)$$

with the initialization

$$\mathcal{R}^C(Q_0) = R_{33}(M). \quad (16)$$

For an elementary S-wave propagating through a sequence of anisotropic layers, the equations for recursive updating of the accumulated normalized R/T coefficient are completely analogous to equations 14–16. On the other hand, if all layers are isotropic, the complete S-wave amplitudes are expressed by the two-component vector

$$\mathbf{U}^{(f)}(R) = \frac{\exp[iT^c(R,S)]}{\mathcal{L}(R,S)}\boldsymbol{\mathcal{R}}^C(Q_K)\boldsymbol{\mathcal{G}}^{(f)}(S;\gamma_1,\gamma_2), \quad (17)$$

where $\boldsymbol{\mathcal{R}}^C$ and $\boldsymbol{\mathcal{G}}^{(f)}$ are 2×2 and 2×1 matrices, respectively. The recursion formula for $\boldsymbol{\mathcal{R}}^C$ is

$$\boldsymbol{\mathcal{R}}^C(Q_k) = \frac{\rho(\tilde{Q}_k)v(\tilde{Q}_k)\cos\psi(\tilde{Q}_k)}{\rho(Q_k)v(Q_k)\cos\psi(Q_k)} \times\mathbf{R}^T(Q_k)\boldsymbol{\mathcal{R}}^C(Q_{k-1})\mathbf{R}(Q_k). \quad (18)$$

All matrices in equation 18 are 2×2.

For a P-wave, the vectorial amplitude function $\mathbf{U}^{(f)}$ is either real valued or purely imaginary, depending entirely on the phase shift attributable to caustics. For S-waves, however, the real and imaginary parts of the vector $\mathbf{U}^{(f)}$ may both be nonzero.

RAY-PROPAGATOR MATRICES

This section reviews the definitions of ray-propagator matrices and two important results for normal-incidence rays obtained by Hubral et al. (1993).

For a ray starting and ending, respectively, at points S and R, a 4×4 ray-propagator matrix has the definition

$$\mathbf{\Pi}(R, S) \equiv \begin{bmatrix} \mathbf{Q}_1(R, S) & \mathbf{Q}_2(R, S) \\ \mathbf{P}_1(R, S) & \mathbf{P}_2(R, S) \end{bmatrix}. \tag{19}$$

The minors of types $\mathbf{Q}$ and $\mathbf{P}$ correspond to the wavefront-orthonormal coordinate system (Červený, 2001), a local Cartesian coordinate system with axes changing continuously along the ray. The system has three orthonormal basis vectors — $\mathbf{e}^{(1)}$, $\mathbf{e}^{(2)}$, and $\mathbf{e}^{(3)}$ — where $\mathbf{e}^{(3)}$ is normal to the wavefront and points in the direction of the slowness vector. For an isotropic medium the wavefront-orthonormal coordinate system coincides with the ray-centered system. The submatrices of the ray-propagator matrix are 2×2 paraxial ray-tracing matrices. Moreover, the sets of matrices $\mathbf{Q}_1$, $\mathbf{P}_1$ and $\mathbf{Q}_2$, $\mathbf{P}_2$ correspond to wavefronts with initial conditions as a plane wave and as a point source, respectively. Some characteristics of the ray-propagator matrix $\mathbf{\Pi}$ are described in Appendix A.

The minors of the ray-propagator matrix $\mathbf{\Pi}(R, S)$ may be projected into local Cartesian coordinate systems associated with interfaces on which points S and R are assumed to be located. The transformations to local interface coordinates lead to the so-called surface-to-surface ray-propagator matrix $\mathbf{T}(R, S)$ (Bortfeld, 1989), with many useful properties and applications (Hubral et al., 1992a, b). The 4×4 surface-to-surface ray-propagator matrix is expressed in terms of four 2×2 submatrices $\mathbf{A}$, $\mathbf{B}$, $\mathbf{C}$, and $\mathbf{D}$:

$$\mathbf{T}(R, S) = \begin{bmatrix} \mathbf{A}(R, S) & \mathbf{B}(R, S) \\ \mathbf{C}(R, S) & \mathbf{D}(R, S) \end{bmatrix}. \tag{20}$$

A summary of the properties of the surface-to-surface ray-propagator matrix is given in Appendix B. Matrix $\mathbf{T}(R, S)$ is related to matrix $\mathbf{\Pi}(R, S)$ by

$$\mathbf{T}(R, S) = \mathbf{Y}(R)\mathbf{\Pi}(R, S)\mathbf{Y}^{-1}(S). \tag{21}$$

The 4×4 matrix $\mathbf{Y}$ describes the projection of paraxial ray coordinates and slowness vector components from the wavefront-orthonormal system to the local-interface system at either S or R. To allow the surface-to-surface propagator matrix $\mathbf{T}(R, S)$ to pertain to arbitrarily anisotropic inhomogeneous media, I use the form of $\mathbf{Y}$ derived by Červený (2001; refer to Appendix C for details).

Let the surface-to-surface ray-propagator matrices corresponding to downward and upward propagation along the normal-incidence ray be denoted as

$$\mathbf{T}(M, S) = \mathbf{T}^{\downarrow} = \begin{bmatrix} \mathbf{A}^{\downarrow} & \mathbf{B}^{\downarrow} \\ \mathbf{C}^{\downarrow} & \mathbf{D}^{\downarrow} \end{bmatrix}, \quad \mathbf{T}(R, M) = \mathbf{T}^{\uparrow} = \begin{bmatrix} \mathbf{A}^{\uparrow} & \mathbf{B}^{\uparrow} \\ \mathbf{C}^{\uparrow} & \mathbf{D}^{\uparrow} \end{bmatrix}. \tag{22}$$

The chain rule in equation B-5 for surface-to-surface ray-propagator matrices yields

$$\mathbf{T}(R, S) = \mathbf{T}^{\uparrow}\mathbf{T}^{\downarrow}. \tag{23}$$

Following Hubral et al. (1993), the matrix $\mathbf{T}(R, S)$ can be expressed alternatively in terms of matrices corresponding to downward propagation,

$$\mathbf{T}(R, S) = \begin{bmatrix} 2\mathbf{D}^{\downarrow T}\mathbf{A}^{\downarrow} - \mathbf{I} & 2\mathbf{B}^{\downarrow T}\mathbf{D}^{\downarrow} \\ 2\mathbf{A}^{\downarrow T}\mathbf{C}^{\downarrow} & 2\mathbf{A}^{\downarrow T}\mathbf{D}^{\downarrow} - \mathbf{I} \end{bmatrix}, \tag{24}$$

or upward propagation,

$$\mathbf{T}(R, S) = \begin{bmatrix} 2\mathbf{A}^{\uparrow}\mathbf{D}^{\uparrow T} - \mathbf{I} & 2\mathbf{A}^{\uparrow}\mathbf{B}^{\uparrow T} \\ 2\mathbf{D}^{\uparrow}\mathbf{C}^{\uparrow T} & 2\mathbf{D}^{\uparrow}\mathbf{A}^{\uparrow T} - \mathbf{I} \end{bmatrix}. \tag{25}$$

In equations 24 and 25, $\mathbf{I}$ is the 2×2 identity matrix.

ONE-WAY EIGENSOLUTION MATRIX FOR THE NORMAL-INCIDENCE RAY

As with the surface-to-surface ray-propagator matrix $\mathbf{T}(R, S)$, it can be useful to express the matrix $\mathbf{\Pi}(R, S)$ solely in terms of paraxial ray-tracing matrices corresponding to integration in one direction along the normal-incidence ray. For upward integration, I introduce in this section the one-way eigensolution matrix.

Applying the chain rule in equation A-6 to the normal-incidence ray, we get

$$\mathbf{\Pi}(R, S) = \mathbf{\Pi}(R, \tilde{M})\mathbf{\Pi}(\tilde{M}, M)\mathbf{\Pi}(M, S), \tag{26}$$

where the interface propagator matrix $\mathbf{\Pi}(\tilde{M}, M)$ is

$$\mathbf{\Pi}(\tilde{M}, M) = \begin{bmatrix} \mathbf{I}^{*} & \mathbf{0} \\ 2c^{-1}(M)\mathcal{D}(M)\mathbf{I}^{*} & \mathbf{I}^{*} \end{bmatrix}. \tag{27}$$

Here, $c(M)$ is the phase velocity in the direction normal to the interface at point M, and $\mathcal{D}(M)$ is the 2×2 interface curvature matrix, given relative to local interface coordinates. The 2×2 matrix $\mathbf{I}^{*}$ has the definition

$$\mathbf{I}^{*} \equiv \begin{bmatrix} -1 & 0 \\ 0 & 1 \end{bmatrix}. \tag{28}$$

The matrix $\mathbf{\Pi}(M, S)$ in equation 26 can be expressed in terms of the minors of matrix $\mathbf{\Pi}(R, \tilde{M})$, using equation A-5 describing back-propagation. The latter minors are subsequently expressed in terms of paraxial ray-tracing matrices associated with the NIP wave and the normal wave. The set of paraxial ray-tracing matrices for the NIP wave is denoted as $\mathbf{Q}_{\mathrm{NIP}}$, $\mathbf{P}_{\mathrm{NIP}}$. Recalling the description of the NIP wave from the introduction, the matrices $\mathbf{Q}_{\mathrm{NIP}}$, $\mathbf{P}_{\mathrm{NIP}}$ must be subjected to point-source initialization at the starting point, which is the point of normal-incidence reflection M. Hence, $\mathbf{Q}_{\mathrm{NIP}}$ and $\mathbf{P}_{\mathrm{NIP}}$ have the definitions

$$\mathbf{Q}_{\mathrm{NIP}}(R) = \mathbf{Q}_2(R, \tilde{M}), \quad \mathbf{P}_{\mathrm{NIP}}(R) = \mathbf{P}_2(R, \tilde{M}). \tag{29}$$

The dynamic ray tracing for the NIP wave must satisfy the initial conditions

$$\mathbf{Q}_{\mathrm{NIP}}(\tilde{M}) = \mathbf{0}, \qquad \mathbf{P}_{\mathrm{NIP}}(\tilde{M}) = \mathbf{I}. \tag{30}$$

Furthermore, let the set of paraxial ray-tracing matrices for the normal wave be denoted as $\mathbf{Q}_N, \mathbf{P}_N$. This set of matrices is similar to the set $\mathbf{Q}_1(R, \tilde{M}), \mathbf{P}_1(R, \tilde{M})$ included in the standard ray-propagator matrix $\mathbf{\Pi}(R, \tilde{M})$ belonging to the upward direction of the normal-incidence ray, with the important distinction that the initialization of $\mathbf{Q}_N, \mathbf{P}_N$ does not rely on an initial plane wave at point M. Rather, $\mathbf{Q}_N, \mathbf{P}_N$ must be initialized such that the curvatures of the wavefront are equal to the curvatures of the NIP interface at M.

At the receiver, the 2×2 matrices of second derivatives of traveltime for the normal wave and the NIP wave are related to the paraxial ray-tracing matrices by

$$\mathbf{M}_N(R) = \mathbf{P}_N(R)\mathbf{Q}_N^{-1}(R), \quad \mathbf{M}_{\text{NIP}}(R) = \mathbf{P}_{\text{NIP}}(R)\mathbf{Q}_{\text{NIP}}^{-1}(R). \tag{31}$$

The corresponding wavefront curvature matrices $\mathbf{K}_N(R)$ and $\mathbf{K}_{\text{NIP}}(R)$ are

$$\mathbf{K}_N(R) = c(R)\mathbf{M}_N(R), \quad \mathbf{K}_{\text{NIP}}(R) = c(R)\mathbf{M}_{\text{NIP}}(R). \tag{32}$$

It is assumed that the local interface coordinate system at point M coincides with the initial wavefront-orthonormal coordinate system defined for upward dynamic ray tracing. Considering equations 31 and 32, the initial conditions for normal-wave dynamic ray tracing can be written

$$\mathbf{Q}_N(\tilde{M}) = \mathbf{I}, \qquad \mathbf{P}_N(\tilde{M}) = c^{-1}(M)\mathcal{D}(M). \tag{33}$$

Thus, after upward propagation we have the result

$$\begin{bmatrix} \mathbf{Q}_N(R) \\ \mathbf{P}_N(R) \end{bmatrix} = \mathbf{\Pi}(R, \tilde{M}) \begin{bmatrix} \mathbf{I} \\ c^{-1}(M)\mathcal{D}(M) \end{bmatrix}. \tag{34}$$

Using equation 34, one can express the paraxial ray-tracing matrices corresponding to an initial plane wavefront at M as follows:

$$\begin{aligned} \mathbf{Q}_1(R, \tilde{M}) &= \mathbf{Q}_N(R) - c^{-1}(M)\mathbf{Q}_{\text{NIP}}(R)\mathcal{D}(M), \\ \mathbf{P}_1(R, \tilde{M}) &= \mathbf{P}_N(R) - c^{-1}(M)\mathbf{P}_{\text{NIP}}(R)\mathcal{D}(M). \end{aligned} \tag{35}$$

By combining equations 26, 27, A-5, and 35, we can eliminate the paraxial ray-tracing matrices $\mathbf{Q}_1(R, \tilde{M})$ and $\mathbf{P}_1(R, \tilde{M})$ from the two-way ray-propagator matrix $\mathbf{\Pi}(R, S)$. The result is

$$\mathbf{\Pi}(R, S) = \begin{bmatrix} \left(2\mathbf{Q}_{\text{NIP}}\mathbf{P}_N^T + \mathbf{I}\right)\mathbf{I}^* & 2\mathbf{Q}_{\text{NIP}}\mathbf{Q}_N^T\mathbf{I}^* \\ 2\mathbf{P}_{\text{NIP}}\mathbf{P}_N^T\mathbf{I}^* & \left(2\mathbf{P}_{\text{NIP}}\mathbf{Q}_N^T - \mathbf{I}\right)\mathbf{I}^* \end{bmatrix}. \tag{36}$$

Equation 36 illustrates that knowledge of the paraxial ray-tracing matrices corresponding to the normal wave and the NIP wave is sufficient to determine the two-way ray-propagator matrix and hence to determine the paraxial ray-tracing matrices of any wavefront considered for two-way propagation along the normal-incidence ray. As a byproduct of the derivation of equation 36, we find that the following relations are invariant along the ray:

$$\begin{aligned} \mathbf{Q}_N\mathbf{P}_{\text{NIP}}^T - \mathbf{Q}_{\text{NIP}}\mathbf{P}_N^T &= \mathbf{I}, & \mathbf{Q}_N\mathbf{Q}_{\text{NIP}}^T - \mathbf{Q}_{\text{NIP}}\mathbf{Q}_N^T &= \mathbf{0}, \\ \mathbf{P}_N\mathbf{P}_{\text{NIP}}^T - \mathbf{P}_{\text{NIP}}\mathbf{P}_N^T &= \mathbf{0}, & \mathbf{P}_{\text{NIP}}\mathbf{Q}_N^T - \mathbf{P}_N\mathbf{Q}_{\text{NIP}}^T &= \mathbf{I}. \end{aligned} \tag{37}$$

In the spirit of Hubral (1983), I define the one-way eigensolution matrix associated with the normal-incidence ray as

$$\mathbf{\Phi}(R, \tilde{M}) \equiv \begin{bmatrix} \mathbf{Q}_N & \mathbf{Q}_{\text{NIP}} \\ \mathbf{P}_N & \mathbf{P}_{\text{NIP}} \end{bmatrix}. \tag{38}$$

Using equation 36 and the invariant relations in equation 37, one can write the two-way ray-propagator matrix in terms of the one-way eigensolution matrix as

$$\mathbf{\Pi}(R, S) \begin{bmatrix} \mathbf{I}^* & \mathbf{0} \\ \mathbf{0} & -\mathbf{I}^* \end{bmatrix} \mathbf{\Phi}(R, \tilde{M}) = \mathbf{\Phi}(R, \tilde{M}) \begin{bmatrix} \mathbf{I} & \mathbf{0} \\ \mathbf{0} & -\mathbf{I} \end{bmatrix}. \tag{39}$$

Equation 39 visualizes an important aspect mentioned by Hubral (1983) — namely, that the NIP wave and the normal wave can be considered as eigensolutions or eigenwavefronts of the normal-incidence ray problem. Considering equation 21 and the equations in Appendix C, it is clear that the one-way eigensolution matrix $\mathbf{\Phi}(R, \tilde{M})$ has a simple relation to the surface-to-surface ray-propagator matrix $\mathbf{T}(R, M)$ corresponding to upward propagation:

$$\mathbf{T}(R, M) = \mathbf{Y}(R)\mathbf{\Phi}(R, \tilde{M}). \tag{40}$$

Thus, the one-way eigensolution matrix can be considered as a special version of the surface-to-surface ray-propagator matrix, for which the surfaces at M and R are, respectively, the NIP interface and a plane perpendicular to the slowness vector at the receiver.

From the ray-propagator matrix in equation 36, one can derive the relations (see Appendix D)

$$\mathbf{Q}_2(R, S) = 2(\mathbf{M}_{\text{NIP}} - \mathbf{M}_N)^{-1}\mathbf{I}^*, \tag{41}$$

$$\mathbf{M}_2(R, S) = \tfrac{1}{2}(\mathbf{M}_{\text{NIP}} + \mathbf{M}_N). \tag{42}$$

Equations 41 and 42 correspond, respectively, to Hubral's (1983) equations 24a and 24b. In the case of rays confined to a plane, Hubral (1983) expresses in his equation 13 a matrix similar to $\mathbf{T}(R, S)$ in terms of the wavefront curvatures (scalars) K_{NIP} and K_N. The corresponding relation for the 3D case is

$$\mathbf{T}(R, S) = \begin{bmatrix} (2(\mathbf{M}_{\text{NIP}} - \mathbf{M}_N)^{-1}\mathbf{M}_N + \mathbf{I})\mathbf{I}^* & 2(\mathbf{M}_{\text{NIP}} - \mathbf{M}_N)^{-1}\mathbf{I}^* \\ 2\mathbf{M}_{\text{NIP}}(\mathbf{M}_{\text{NIP}} - \mathbf{M}_N)^{-1}\mathbf{M}_N\mathbf{I}^* & (2\mathbf{M}_{\text{NIP}}(\mathbf{M}_{\text{NIP}} - \mathbf{M}_N)^{-1} - \mathbf{I})\mathbf{I}^* \end{bmatrix}. \tag{43}$$

DETERMINATION OF SEISMIC ATTRIBUTES

In the following we determine seismic attributes based on numerical integration in one direction along the normal-incidence ray, using either the surface-to-surface ray-propagator matrix formulation or the one-way eigensolution formulation. An important basis for this section is the fact that the two-way surface-to-surface ray-propagator matrix $\mathbf{T}(R, S)$ can be expressed in terms of submatrices of the one-way matrices $\mathbf{T}^{\downarrow}$ and $\mathbf{T}^{\uparrow}$ by equations 24 and 25. The standard two-way ray-propagator matrix $\mathbf{\Pi}(R, S)$ is, on the other hand, given by equation 36 in terms of the submatrices of the one-way eigensolution matrix $\mathbf{\Phi}$.

Relative geometric spreading

Consider the relative geometric spreading $\mathcal{L}(R, S)$ included in equation 2 for the seismic amplitude function. The relative geometric spreading is defined as

$$\mathcal{L}(R, S) = |\det \mathbf{Q}_2(R, S)|^{1/2}. \tag{44}$$

Looking at the relative geometric spreading in the perspective of surface-to-surface ray-propagator theory, we can use the result

$$\mathcal{L}(R, S) = \frac{v(R)}{c(R)} \cos\psi(R)\ |\det \mathbf{B}(R, S)|^{1/2}, \tag{45}$$

obtained by Schleicher et al. (2001) (see also Appendix C). For isotropic conditions at the common source/receiver, the group and phase velocities are equal, and the angle of incidence of the group velocity vector (group angle ψ) equals the angle of incidence of the slowness vector (phase angle φ). This gives

$$\mathcal{L}(R, S) = \cos\varphi(R)\ |\det \mathbf{B}(R, S)|^{1/2}\ . \tag{46}$$

The calculation of the determinant of the matrix $\mathbf{B}(R, S)$ can be based alternatively on the submatrices of the matrices $\mathbf{T}^{\downarrow}$ or $\mathbf{T}^{\uparrow}$ since, from equations 24 and 25, we have

$$\mathbf{B}(R, S) = 2\mathbf{B}^{\downarrow T}\mathbf{D}^{\downarrow}, \qquad \mathbf{B}(R, S) = 2\mathbf{A}^{\uparrow}\mathbf{B}^{\uparrow T}. \tag{47}$$

In dynamic ray tracing, matrix types $\mathbf{A}$, $\mathbf{B}$, $\mathbf{C}$, and $\mathbf{D}$ occur in pairs as the sets $\mathbf{A}, \mathbf{C}$ and $\mathbf{B}, \mathbf{D}$. Therefore, one can observe that the set of paraxial ray-tracing matrices $\mathbf{B}^{\downarrow}, \mathbf{D}^{\downarrow}$ is sufficient to obtain $\mathcal{L}(R, S)$ if dynamic ray tracing is performed in the downward direction of the normal-incidence ray. In the case of upward integration, two sets of paraxial ray-tracing matrices ($\mathbf{A}^{\uparrow}, \mathbf{C}^{\uparrow}$ and $\mathbf{B}^{\uparrow}, \mathbf{D}^{\uparrow}$) are required.

On the other hand, we have from equation 36 that the paraxial ray-tracing matrix $\mathbf{Q}_2(R, S)$ can be obtained by

$$\mathbf{Q}_2(R, S) = 2\mathbf{Q}_{\mathrm{NIP}}\mathbf{Q}_N^T\mathbf{I}^*. \tag{48}$$

Thus, the relative geometric spreading for the reflected wave can be computed from the simple formula

$$\mathcal{L}(R, S) = 2\mathcal{L}_{\mathrm{NIP}}\mathcal{L}_N. \tag{49}$$

On the right-hand side of equation 49, we find the geometric spreading corresponding to the NIP wave and the normal wave:

$$\mathcal{L}_{\mathrm{NIP}} = |\det \mathbf{Q}_{\mathrm{NIP}}|^{1/2}, \qquad \mathcal{L}_N = |\det \mathbf{Q}_N|^{1/2}\ . \tag{50}$$

Fresnel zone matrix

The next attribute to be considered is the Fresnel zone matrix for the NIP interface. Let f denote the frequency of a harmonic wave. We establish a local coordinate system with coordinates (z_1, z_2, z_3) at the normal-incidence point M, with the z_3-axis normal to the interface. Furthermore, a two-component vector $\bar{\mathbf{z}} = (z_1, z_2)^T$ is defined to contain only the tangential components of position with respect to the interface. The projected Fresnel zone on the NIP interface corresponding to the frequency f is then

$$|\bar{\mathbf{z}}^T\mathbf{M}^F\bar{\mathbf{z}}| = f^{-1}, \tag{51}$$

where the 2×2 matrix $\mathbf{M}^F$ is the Fresnel zone matrix.

Hubral et al. (1993) derive the following expressions for the Fresnel zone matrix:

$$\mathbf{M}^F = 2\mathbf{D}^{\downarrow}\mathbf{B}^{\downarrow -1}, \qquad \mathbf{M}^F = 2\mathbf{B}^{\uparrow -1}\mathbf{A}^{\uparrow}. \tag{52}$$

The formulas in equation 52 are valid for isotropic and anisotropic media if appropriate projections are used (Appendix C). For downward and upward propagation, the matrix $\mathbf{B}(R, S)$ can be decomposed by

$$\mathbf{B}(R, S) = \mathbf{B}^{\downarrow T}\mathbf{M}^F\mathbf{B}^{\downarrow}, \qquad \mathbf{B}(R, S) = \mathbf{B}^{\uparrow}\mathbf{M}^F\mathbf{B}^{\uparrow T}. \tag{53}$$

The Fresnel zone matrix can be expressed in terms of the $\mathbf{Q}$ matrices for the NIP wave and the normal wave as

$$\mathbf{M}^F = 2\mathbf{Q}_{\mathrm{NIP}}^{-1}\mathbf{Q}_N. \tag{54}$$

The matrix $\mathbf{Q}_2(R, S)$ is decomposed with respect to the matrices $\mathbf{Q}_{\mathrm{NIP}}$ and $\mathbf{M}^F$ by

$$\mathbf{Q}_2(R, S) = \mathbf{Q}_{\mathrm{NIP}}\mathbf{M}^F\mathbf{Q}_{\mathrm{NIP}}^T\mathbf{I}^*. \tag{55}$$

Phase shift from caustics

The phase shift $T^c(R, S)$ from caustics in equation 2 is given by

$$T^c(R, S) = -k(R, S)\frac{\pi}{2}. \tag{56}$$

The quantity $k(R, S)$ is the KMAH index, defined as the total number of elementary caustics passed between points S and R. The term, introduced by Ziolkowki and Deschamps (1980), acknowledges the work of Keller, Maslov, Arnold, and Hörmander. Kravtsov and Orlov (1980) use the term index of the ray trajectory. The theory for decomposition of the KMAH index (Goldin, 1991; Goldin and Piankov, 1992; Hubral et al., 1992b; Schleicher et al., 1993a), and equation 55 for the decomposition of the matrix $\mathbf{Q}_2(R, S)$ yield the KMAH index for the reflected wave as

$$k(R, S) = 2k_{\mathrm{NIP}} + k^F(M). \tag{57}$$

Here, k_{NIP} is the KMAH index for the NIP wave and $k^F(M)$ can be obtained by

$$k^F(M) = \tfrac{1}{2}[2 - \mathrm{Sgn}\mathbf{M}^F(M; R, S)]. \tag{58}$$

The signature $\mathrm{Sgn}\mathbf{M}^F$ represents the number of positive eigenvalues minus the number of negative eigenvalues. As pointed out by Červený (2001, 383–384), one also can write

$$\mathrm{Sgn}\mathbf{M}^F = \mathrm{Sgn}M_1 + \mathrm{Sgn}M_2, \tag{59}$$

where M_1 and M_2 denote the two eigenvalues of the Fresnel zone matrix. Thus, the KMAH index for the reflected wave can be computed by checking the KMAH index for the NIP wave during the upward propagation toward the receiver, followed by calculation of the term $k^F(M)$ once R has been reached.

Equation 48 shows that the KMAH index for the reflected wave can be expressed alternatively as the sum

$$k(R, S) = k_N + k_{\mathrm{NIP}}, \tag{60}$$

where k_N is the KMAH index for the normal wave. Thus, $k^F(M)$ can be reformulated as

$$k^F(M) = k_N - k_{\text{NIP}}. \tag{61}$$

The KMAH index for a wave originating as a point source is reciprocal (Klimeš, 1997). This makes equations 57 and 60 also applicable to elementary S-waves in anisotropic media, for which a so-called anomalous phase shift may occur at the source. Klimeš (1997) and Bakker (1998) give mathematical recipes for how the KMAH index can be computed along a ray in an anisotropic model.

NMO velocity

The hyperbolic aproximation to the traveltime function of the CMP domain is

$$T^2_{\text{CMP}}(R, S) = T_0^2 + \frac{r^2}{v^2_{\text{NMO}}(\theta)}. \tag{62}$$

Here, T_0 is the two-way zero-offset traveltime, r is the source-receiver offset, and θ denotes the azimuth of the line profile under consideration. Following Hubral et al. (1993), the squared NMO velocity can be expressed as

$$v^2_{\text{NMO}}(\theta) = \frac{2}{T_0 \bar{\mathbf{e}}^T(\theta)\mathbf{M}^{(x)}\bar{\mathbf{e}}(\theta)}, \tag{63}$$

where the 2×2 matrix $\mathbf{M}^{(x)}$ is related to the minors of the matrices $\mathbf{T}^{\downarrow}$ and $\mathbf{T}^{\uparrow}$ as follows (Schleicher et al., 1993b):

$$\mathbf{M}^{(x)} = \mathbf{B}^{\downarrow -1}\mathbf{A}^{\downarrow}, \qquad \mathbf{M}^{(x)} = \mathbf{D}^{\uparrow}\mathbf{B}^{\uparrow -1}. \tag{64}$$

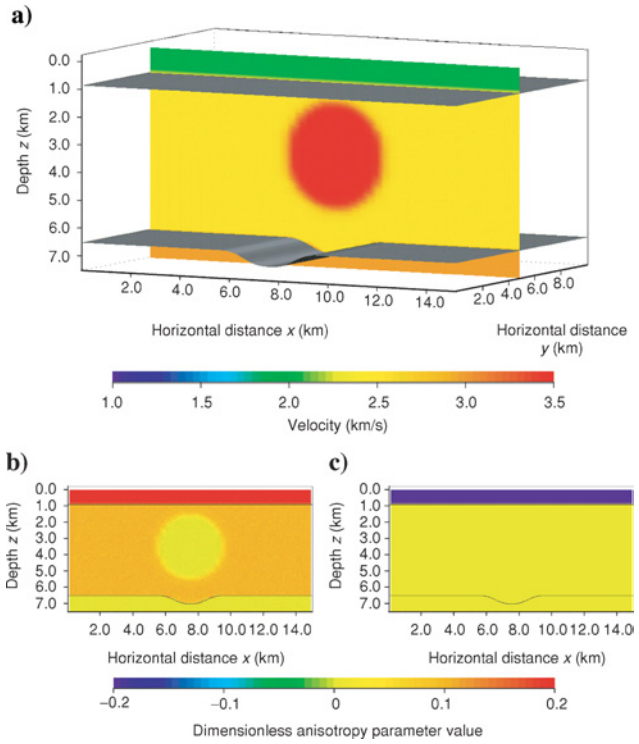

Figure 3. Velocity model for numerical examples. A cross section at horizontal coordinate $y = 5.0$ km is shown for (a) vertical P-wave phase velocity, (b) Thomsen's parameter ϵ, and (c) Thomsen's parameter δ. The model is truly 3D since the high-velocity region is spherical.

A proof is included in Appendix E. The two-component unit vector $\bar{\mathbf{e}}(\theta)$ in equation 63 has the definition

$$\bar{\mathbf{e}}(\theta) = (\cos\theta, \sin\theta)^T. \tag{65}$$

Equation 63 is valid for isotropic and anisotropic models. For anisotropic conditions at sources and receivers distributed on a planar and horizontal surface, the projection formula for the matrix $\mathbf{M}_{\text{NIP}}$ is

$$\mathbf{M}^{(x)} = \mathbf{E}(R) + [\mathbf{G}(R) - \mathbf{A}^{an}(R)]\mathbf{M}_{\text{NIP}}\,[\mathbf{G}(R) - \mathbf{A}^{an}(R)]^T. \tag{66}$$

For a definition of the quantities in equation 66, see Appendix C.

The hyperbolic approximation in equation 62 is exact for a homogeneous isotropic medium but is generally inadequate for large source-receiver offsets in anisotropic media. To attain better accuracy and provide a more relevant basis for velocity analysis, equation 62 is expanded to the fourth order (Tsvankin and Thomsen, 1994) and higher. In such nonhyperbolic approximations, the NMO velocity given by equation 63 has a role even in the higher-order terms, e.g., in the quartic coefficient.

NUMERICAL EXAMPLES

The recursive approach that permits the amplitude of the reflected wave to be obtained solely by upward calculations along the normal-incidence ray has been implemented for 3D layered models with vertical polar anisotropy in the layers. In the following, examples are shown that demonstrate the applicability of this one-way amplitude-modeling method.

The model coordinates are referred to in this section as x, y, and z. Consider a velocity model consisting of three main layers (Figure 3) separated by two interfaces. The upper interface is a horizontal plane; the lower interface is shaped as a syncline with no variation in the y-direction. The upper layer is homogeneous, with parameters $V_P = 2.0$ km/s, $\epsilon = 0.2$, and $\delta = -0.2$. In the middle layer is a spherical body with high P-wave velocity (3.5 km/s) and isotropic conditions. The region outside the sphere has vertical P-wave velocity of 2.5 km/s and anisotropic parameter values of $\epsilon = 0.1$, and $\delta = 0$. The lower layer is isotropic with P-wave velocity of 3.0 km/s. In the entire model, the vertical S-wave velocity V_S is set to $V_P/\sqrt{3}$, while the anisotropy parameter γ is set to zero. I also made an isotropic version of this velocity model ($\epsilon = \delta = \gamma = 0$ everywhere).

Four experiments were conducted, corresponding to P- and S-wave propagation for the isotropic and the anisotropic models. The results are shown in Figures 4–7. In each experiment, the wavefront construction method was used initially to find the arrivals. Based on these arrivals, normal-incidence rays were traced between the NIP interface and the given source/receiver locations. Thereafter, the recursive one-way approach was applied along each ray to compute amplitude coefficients and synthetic seismograms.

The sources/receivers were chosen to be along the line $y = 5.0$ km. Because of the symmetry of the velocity model with respect to the plane $y = 5.0$ km, all rays were, in principle, confined to this plane. The motivation for setting up the experiments in this way was twofold. First, a simple example of the recursive algorithm could be made for S-waves exposed to

anisotropic conditions. The direction of the initial single force and the direction of the recording axis were both defined to be along the *x*-axis of the model coordinate system. By this setup, the S-wave propagation was exclusively SV made; there was no conversion to the SH mode at the interfaces encountered along the rays. For the P-wave simulations, the initial force and the recording component were both chosen along the z-axis. Second, the two model versions and the survey setup were designed to create a prominent number of caustics and multiple arrivals. In the isotropic model, multiple arrivals arise because of the syncline-shaped NIP interface and the high velocity contrast between the sphere and its surroundings. The same type of multiple arrivals appears for P-wave rays in the anisotropic model. For the anisotropic model, the S-waves are also subjected to multipathing in the upper layer because of the concavity of the slowness surface.

In all four sections (Figures 4–7), the central triplication is caused by the NIP interface, while the two side triplications are generated by the large velocity contrast in the middle layer. The late arrivals of the central triplication have a phase shift of 90° relative to the earlier arrivals. On the other hand, the late arrivals of the side triplications have a phase shift of 180°. The reason for this difference is that the late arrivals of the side triplications have been exposed to a caustic twice — one on the way down, one on the way up. We can observe that the left- and right-most dipping events arrive earlier for the anisotropic model than for the isotropic model.

The validity of the theory and implementation of the one-way approach was checked by performing the amplitude calculation as a two-way process with point-source initialization at the source/receiver. In all four experiments, acceptable consistency was achieved for the modulus as well as for the phase of the amplitude coefficient, which is shown in Figure 8 for P-wave rays in the anisotropic model (Figure 5). The real and imaginary parts of the complex-valued amplitude coefficient in equation 14 were computed by the one-way approach (Figure 8a) and by two-way dynamic ray tracing. Figure 8b shows the discrepancies in estimated real and imaginary parts of the amplitude coefficient, expressed as a percentage of the one-way result. For most of the events, the amplitude difference is less than 0.25%, and the difference exceeds 0.5% only in two cases, where we find the receiver located very close to a caustic. Since the standard ray method is generally known to give unreliable amplitudes in the vicinity of a caustic, one should not give too much attention to inconsistencies between the one- and two-way amplitude-estimation approaches in such regions.

DISCUSSION

Hubral et al. (1993) point out that the calculation of geometric spreading and phase shift resulting from caustics should be done in either the upward or downward direction and not by a two-way round trip along the normal-incidence ray. The cal-

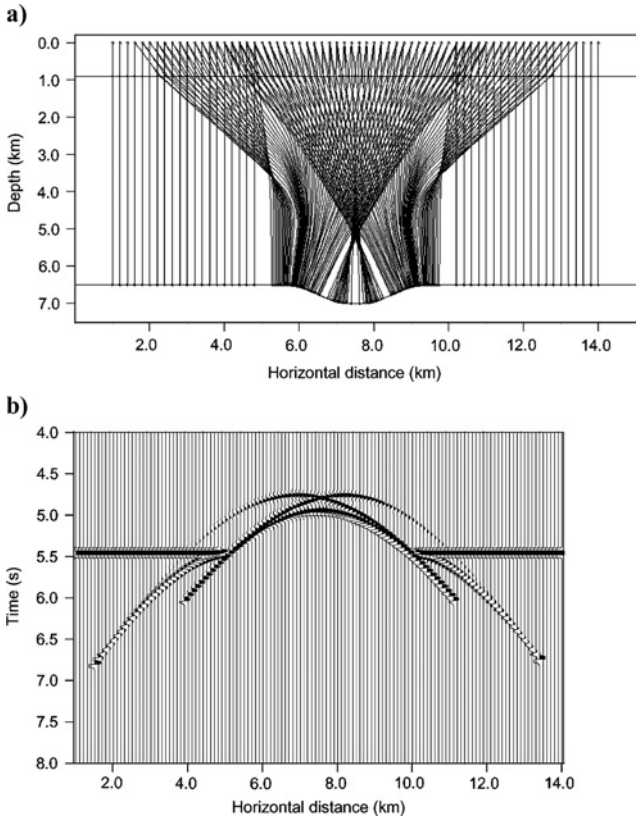

Figure 4. (a) Rays and (b) seismograms for reflected PP-waves for the isotropic model. The initial force and the recording direction are along the vertical axis. Rays are plotted for every second trace.

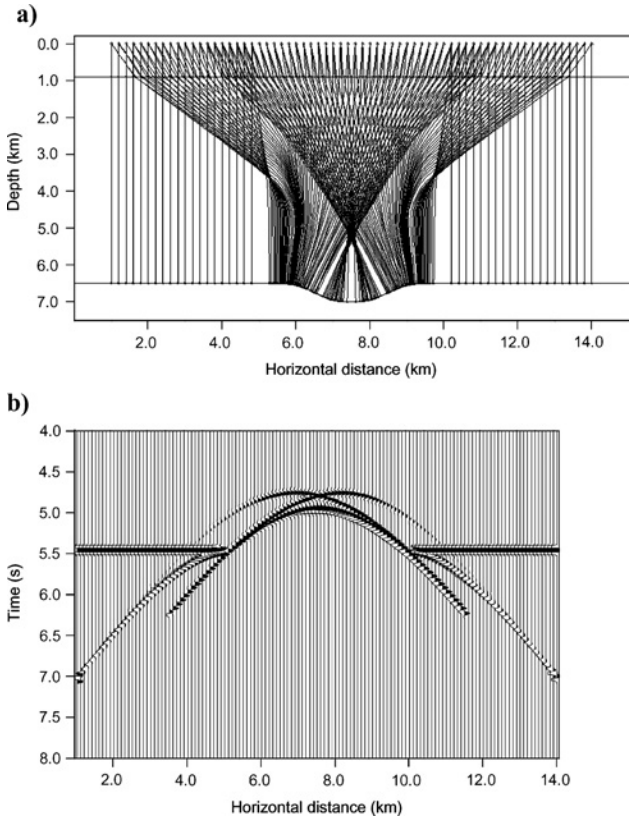

Figure 5. (a) Rays and (b) seismograms for reflected PP-waves for the anisotropic model. The initial force and the recording direction are along the vertical axis. Rays are plotted for every second trace.

culation of the reflected-wave amplitude coefficient was, however, outlined as a two-way process. By utilizing the reciprocal property of normalized R/T matrices (Červený, 2001), we see that the calculation of the accumulated normalized R/T coefficients for reflected P- and S-waves can be formulated as a one-way recursion process.

The surface-to-surface ray-propagator matrix $\mathbf{T}^{\uparrow}$ for upward propagation along the normal-incidence ray is commonly computed by dynamic ray tracing in terms of the standard ray-propagator matrix $\mathbf{\Pi}^{\uparrow}$, followed by projections to the NIP interface and to the surface of source/receiver locations. The matrix $\mathbf{T}^{\uparrow}$ can alternatively be computed as the product of the one-way eigensolution matrix $\mathbf{\Phi}$ and a projection matrix belonging to the receiver location. The minors of the one-way eigensolution matrix are paraxial ray-tracing matrices for the normal wave and the NIP wave, and the formulas for the relative geometric spreading, the KMAH index, and the Fresnel zone matrix become particularly simple if expressed in terms of these minors. Another consequence is that the reflected-wave amplitude and the Fresnel zone matrix can be calculated at the receiver without explicit knowledge of the interface curvature matrix. The reason is that the effect of the interface curvatures is completely embedded in the paraxial ray-tracing matrices belonging to the normal wave. This property is expected to be important in zero-offset modeling by one-way wavefront construction since it eliminates the need for accessing parameters of the NIP interface at the stage of calculating attributes in the receivers.

Dynamic ray tracing based on the one-way eigensolution matrix opens up two possibilities for calculating the KMAH index for the reflected wave. The approach described by Hubral et al. (1993) implies checking the KMAH index for the NIP wave along the ray and calculating the signature of the Fresnel zone matrix once an event has been obtained in a receiver. An alternative computation is based on the result that the KMAH index for the reflected wave is the sum of the KMAH indices corresponding to the normal wave and the NIP wave. Having two such approaches available provides the possibility of verifying that the KMAH index calculation is correct and consistent.

When merging the formulas in Červený (2001) for amplitude calculation for isotropic and anisotropic structures into equation 2, it is important to be aware of the meaning of the S-wave amplitude coefficients that will be computed for a given ray. The reason is that the amplitude coefficients of S-wave ray tracing for anisotropic structures pertain to one of the elementary S-waves (S1 or S2), whereas the amplitude coefficients for isotropic structures correspond to all possible combinations of such waves. For isotropic structures the elementary wave modes S1 and S2 always have equal traveltimes, which is not the case for anisotropic structures because of shear-wave splitting. To include all S-wave combinations for anisotropic

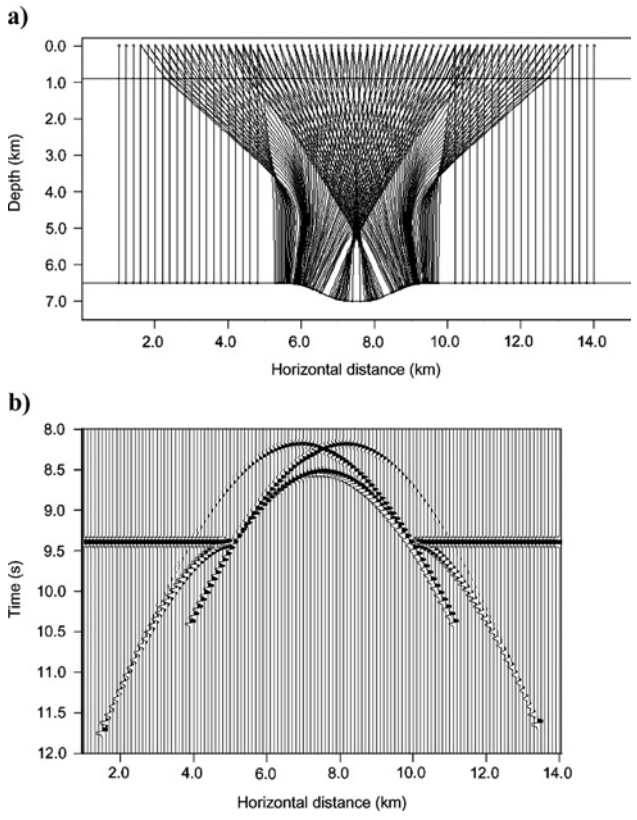

Figure 6. (a) Rays and (b) seismograms for reflected SS-waves for the isotropic model. The initial force and the recording direction are along the horizontal axis. Rays are plotted for every second trace.

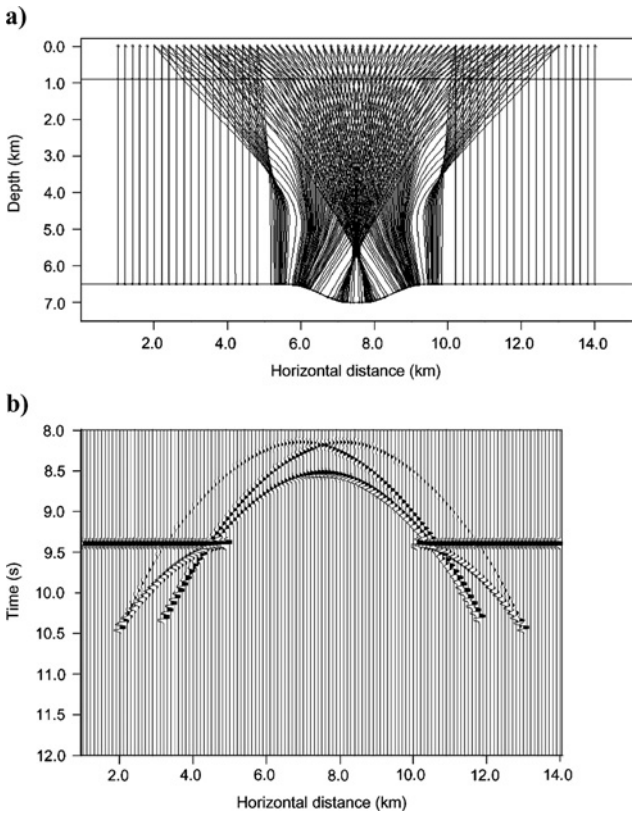

Figure 7. (a) Rays and (b) seismograms for reflected SS-waves for the anisotropic model. The initial force and the recording direction are along the horizontal axis. Rays are plotted for every second trace.

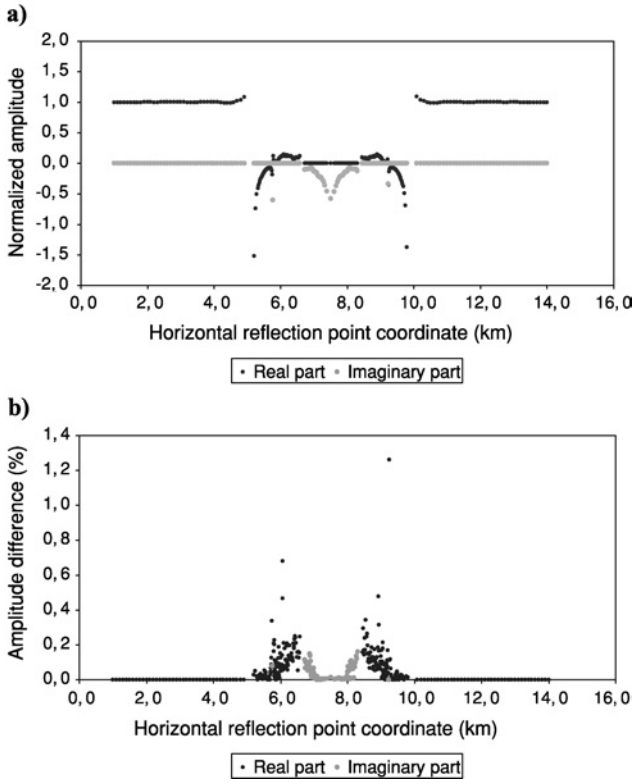

Figure 8. (a) P-wave amplitude coefficient corresponding to the rays and seismograms in Figure 5 plotted versus the horizontal coordinate of the reflection point. The amplitudes have been normalized by the value obtained for the flat parts of the syncline-shaped interface. (b) Discrepancy in percent of the amplitude coefficient estimated by two-way dynamic ray tracing relative to the amplitude coefficient estimated by one-way dynamic ray tracing.

media, one must, in principle, trace one ray for each combination. The quasi-isotropic approximation (Coates and Chapman, 1990; Pšenčík, 1998; Pšenčík and Dellinger, 2001) and the common anisotropic ray approximation (Bakker, 2002; Bulant and Klimeš, 2002) are introduced with the intention to make the computations of S-wave amplitudes less complicated, more efficient, and more robust. Such approximations have not been considered in this paper, but the presented theory forms a basis for possible future extensions, taking into account frequency-dependent S-wave coupling.

CONCLUDING REMARKS

The well-established theory of normal-incidence rays is generalized to include P- and S-waves in isotropic layers as well as P-waves and elementary S-waves in anisotropic layers. The theory has been formulated in such a way that the three main parameters contributing to the amplitude of the reflected wave (geometric spreading, phase shift from caustics, and accumulated normalized R/T coefficients) can be propagated step by step from the NIP interface toward the coinciding sources/receivers. This recursive formulation prepares the ground for implementing zero-offset amplitude modeling as a one-way wavefront construction process.

ACKNOWLEDGMENTS

This work has been inspired by the publications of Peter Hubral and coworkers. The author thanks NORSAR for the opportunity to publish the results in GEOPHYSICS. In particular, appreciation goes to Håvar Gjøystdal, who introduced the author to the theory of normal-incidence rays in the early 1980s and also reviewed the first version of the manuscript. The author is grateful to Claudia Vanelle, Boris Kashtan, and two anonymous reviewers for their enthusiasm and useful suggestions. This work received support from the Research Council of Norway (project 163390/S30).

APPENDIX A

PROPERTIES OF THE STANDARD RAY-PROPAGATOR MATRIX

This appendix summarizes some essential properties of a 4×4 ray-propagator matrix $\mathbf{\Pi}$. The ray-propagator matrix is symplectic, which means that the property

$$\mathbf{\Pi}^T \begin{bmatrix} \mathbf{0} & \mathbf{I} \\ -\mathbf{I} & \mathbf{0} \end{bmatrix} \mathbf{\Pi} = \begin{bmatrix} \mathbf{0} & \mathbf{I} \\ -\mathbf{I} & \mathbf{0} \end{bmatrix} \tag{A-1}$$

is satisfied in all points along the ray. Equation A-1 implies that the inverse of the ray-propagator matrix is

$$\mathbf{\Pi}^{-1} = \begin{bmatrix} \mathbf{P}_2^T & -\mathbf{Q}_2^T \\ -\mathbf{P}_1^T & \mathbf{Q}_1^T \end{bmatrix}. \tag{A-2}$$

The ray-propagator matrix has determinant equal to one. A number of relations, including the minors of the ray-propagator matrix, are invariant along the ray, e.g.,

$$\begin{aligned} \mathbf{Q}_1\mathbf{P}_2^T - \mathbf{Q}_2\mathbf{P}_1^T &= \mathbf{I}, \qquad & \mathbf{Q}_1\mathbf{Q}_2^T - \mathbf{Q}_2\mathbf{Q}_1^T &= \mathbf{0}, \\ \mathbf{P}_1\mathbf{P}_2^T - \mathbf{P}_2\mathbf{P}_1^T &= \mathbf{0}, \qquad & \mathbf{P}_2\mathbf{Q}_1^T - \mathbf{P}_1\mathbf{Q}_2^T &= \mathbf{I}. \end{aligned} \tag{A-3}$$

Given that the forward direction of propagation is defined as the direction from point S to point R, one can write the ray-propagator matrix corresponding to back propagation (from R to S), with the third axis of the wavefront-orthonormal system pointing in this direction, as

$$\mathbf{\Pi}(S, R) = \begin{bmatrix} \mathbf{I}^* & \mathbf{0} \\ \mathbf{0} & -\mathbf{I}^* \end{bmatrix} \mathbf{\Pi}^{-1}(R, S) \begin{bmatrix} \mathbf{I}^* & \mathbf{0} \\ \mathbf{0} & -\mathbf{I}^* \end{bmatrix}. \tag{A-4}$$

The inverse $\mathbf{\Pi}^{-1}(R, S)$ and the 2×2 matrix $\mathbf{I}^*$ are given by equations A-2 and 28, respectively. From equation A-4 one can write the ray-propagator matrix corresponding to backward tracing compactly as

$$\mathbf{\Pi}(S, R) = \begin{bmatrix} \mathbf{I}^*\mathbf{P}_2^T(R, S)\mathbf{I}^* & \mathbf{I}^*\mathbf{Q}_2^T(R, S)\mathbf{I}^* \\ \mathbf{I}^*\mathbf{P}_1^T(R, S)\mathbf{I}^* & \mathbf{I}^*\mathbf{Q}_1^T(R, S)\mathbf{I}^* \end{bmatrix}. \tag{A-5}$$

For a ray intersecting K interfaces at points $Q_1, Q_2, \ldots, Q_K$ between points S and R, the ray-propagator matrix can be

chained as follows:

$$\begin{aligned}\mathbf{\Pi}(R, S) = {} & \mathbf{\Pi}(R, \tilde{Q}_K)\mathbf{\Pi}(\tilde{Q}_K, Q_K)\mathbf{\Pi}(Q_K, \tilde{Q}_{K-1}) \\ & \times \mathbf{\Pi}(\tilde{Q}_{K-1}, Q_{K-1}) \\ & \cdots \times \mathbf{\Pi}(Q_2, \tilde{Q}_1)\mathbf{\Pi}(\tilde{Q}_1, Q_1)\mathbf{\Pi}(Q_1, S).\end{aligned} \tag{A-6}$$

A type $\mathbf{\Pi}(\tilde{Q}_k, Q_k)$ matrix is called an interface propagator matrix. Equation A-6 is the chain rule of ray-propagator matrices.

By invoking the reciprocity principle (Hubral, 1983), one can utilize that the ray-propagator matrix corresponding to two-way propagation along the normal-incidence ray must remain the same if we interchange source and receiver as well as the direction of the ray. Thus,

$$\mathbf{\Pi}(R, S) = \mathbf{\Pi}(S, R), \tag{A-7}$$

where $\mathbf{\Pi}(S, R)$ is given by equation A-5. A consequence of the reciprocity relation A-7 is that

$$\mathbf{Q}_1(R, S) = \mathbf{I}^*\mathbf{P}_2(R, S)^T\mathbf{I}^*. \tag{A-8}$$

Moreover, the matrix products $\mathbf{Q}_2(R, S)\mathbf{I}^*$ and $\mathbf{P}_1(R, S)\mathbf{I}^*$ are symmetric. These symmetry properties are not generally valid; they pertain specifically to two-way tracing along normal-incidence rays.

APPENDIX B

PROPERTIES OF THE SURFACE-TO-SURFACE RAY-PROPAGATOR MATRIX

Properties of a 4×4 surface-to-surface ray-propagator matrix $\mathbf{T}$ are described in this appendix. As with the standard ray-propagator matrix, the surface-to-surface ray-propagator matrix is symplectic, which yields the inverse

$$\mathbf{T}^{-1} = \begin{bmatrix} \mathbf{D}^T & -\mathbf{B}^T \\ -\mathbf{C}^T & \mathbf{A}^T \end{bmatrix}. \tag{B-1}$$

The relations

$$\begin{aligned} \mathbf{A}\mathbf{D}^T - \mathbf{B}\mathbf{C}^T &= \mathbf{I}, \qquad & \mathbf{A}\mathbf{B}^T - \mathbf{B}\mathbf{A}^T &= \mathbf{0}, \\ \mathbf{C}\mathbf{D}^T - \mathbf{D}\mathbf{C}^T &= \mathbf{0}, \qquad & \mathbf{D}\mathbf{A}^T - \mathbf{C}\mathbf{B}^T &= \mathbf{I}, \end{aligned} \tag{B-2}$$

are invariant along a ray. For tracing in the backward direction (from R to S), the surface-to-surface propagator matrix is

$$\mathbf{T}(S, R) = \begin{bmatrix} \mathbf{I} & \mathbf{0} \\ \mathbf{0} & -\mathbf{I} \end{bmatrix} \mathbf{T}^{-1}(R, S) \begin{bmatrix} \mathbf{I} & \mathbf{0} \\ \mathbf{0} & -\mathbf{I} \end{bmatrix}. \tag{B-3}$$

Insertion of the inverse matrix given by equation B-1 yields the compact expression

$$\mathbf{T}(S, R) = \begin{bmatrix} \mathbf{D}^T(R, S) & \mathbf{B}^T(R, S) \\ \mathbf{C}^T(R, S) & \mathbf{A}^T(R, S) \end{bmatrix}. \tag{B-4}$$

For a ray intersecting N interfaces between points S and R, the chain rule for surface-to-surface ray-propagator matrices is

$$\begin{aligned}\mathbf{T}(R, S) = {} & \mathbf{T}(R, Q_N)\mathbf{T}(Q_N, Q_{N-1}) \\ & \times \cdots \mathbf{T}(Q_2, Q_1)\mathbf{T}(Q_1, S).\end{aligned} \tag{B-5}$$

No interface-propagator matrix is included in the terminology of surface-to-surface ray-propagator matrices.

The matrix $\mathbf{T}(R, S)$ for two-way propagation along the normal-incidence ray satisfies the reciprocity relation

$$\mathbf{T}(R, S) = \mathbf{T}(S, R), \tag{B-6}$$

where $\mathbf{T}(S, R)$ is given by equation B-4. From equation B-6 one can conclude that

$$\mathbf{A}(R, S) = \mathbf{D}^T(R, S) \tag{B-7}$$

and that matrices $\mathbf{B}(R, S)$ and $\mathbf{C}(R, S)$ are symmetric. Equation B-7 corresponds directly to Hubral's (1983) condition $A = D$, valid for a normal-incidence ray in a 2D medium.

APPENDIX C

RELATING GEOMETRIC SPREADING TO RAY-PROPAGATOR MATRICES

The connection between the standard ray-propagator matrix $\mathbf{\Pi}$ and the surface-to-surface ray-propagator matrix $\mathbf{T}$ and their relations to geometric spreading are addressed in this appendix. For a ray between two points S and R, the equation linking the two 4×4 matrices $\mathbf{T}$ and $\mathbf{\Pi}$ is

$$\mathbf{T}(R, S) = \mathbf{Y}(R)\mathbf{\Pi}(R, S)\mathbf{Y}^{-1}(S). \tag{C-1}$$

The 4×4 matrix $\mathbf{Y}$ has the form

$$\mathbf{Y} = \begin{bmatrix} (\mathbf{G} - \mathbf{A}^{an})^{-1^T} & \mathbf{0} \\ (\mathbf{E} - p_3^{(z)}\mathcal{D})(\mathbf{G} - \mathbf{A}^{an})^{-1^T} & (\mathbf{G} - \mathbf{A}^{an}) \end{bmatrix}. \tag{C-2}$$

The various quantities in equation C-2 are explained in the following; see also Červeň (2001, 411–414). The scalar $p_3(z)$ is the component of the slowness vector with respect to the third coordinate axis of the local interface system. This coordinate axis is perpendicular to the interface at the point under consideration (S, R, or some other point on the ray). The 2×2 matrices $\mathbf{E}$ and $\mathbf{A}^{an}$ are, respectively, the inhomogeneity matrix and anisotropy matrix, with elements given by

$$\begin{aligned}\mathbf{E}_{IJ} = {} & c^{-1}\big[G_{I3}G_{JM}\eta_M^{(y)} + G_{J3}G_{IK}\eta_K^{(y)} \\ & + G_{I3}G_{J3}\big(\eta_3^{(y)} - c^{-1}\eta_L^{(y)}v_L^{(y)}\big)\big],\end{aligned} \tag{C-3}$$

$$\mathbf{A}_{IJ}^{an} = p_I^{(z)}v_J^{(y)}. \tag{C-4}$$

The inverse of $\mathbf{Y}$ is

$$\mathbf{Y}^{-1} = \begin{bmatrix} (\mathbf{G} - \mathbf{A}^{an})^T & \mathbf{0} \\ -(\mathbf{G} - \mathbf{A}^{an})^{-1}\big(\mathbf{E} - p_3^{(z)}\mathcal{D}\big) & (\mathbf{G} - \mathbf{A}^{an})^{-1} \end{bmatrix}. \tag{C-5}$$

The matrix $\mathbf{G}$ is the upper-left 2×2 submatrix of the 3×3 matrix $\hat{\mathbf{G}}$ that describes rotation from wavefront-orthonormal coordinates to local interface coordinates.

In the case of a two-way normal-incidence raypath, the matrices $\mathbf{Y}(S)$ and $\mathbf{Y}(R)$ are related through the transformation

$$\mathbf{Y}(S) = \mathbf{Y}(R) \begin{bmatrix} \mathbf{I}^* & \mathbf{0} \\ \mathbf{0} & \mathbf{I}^* \end{bmatrix}. \tag{C-6}$$

With the help of equations C-1, C-2, C-5, and C-6, we can express the 2×2 matrix $\mathbf{B}(R, S)$ in terms of the 2×2 matrix $\mathbf{Q}_2(R, S)$:

$$\mathbf{B}(R, S) = -(\mathbf{G} - \mathbf{A}^{an})^{-1^T} \mathbf{Q}_2(R, S)\mathbf{I}^*(\mathbf{G} - \mathbf{A}^{an})^{-1}. \tag{C-7}$$

The corresponding determinants are related by the equation

$$\det \mathbf{B}(R, S) = \frac{\det \mathbf{Q}_2(R, S)}{[\det(\mathbf{G} - \mathbf{A}^{an})]^2}. \tag{C-8}$$

By examining the nature of the transformation matrix $\mathbf{G}-\mathbf{A}^{an}$, one finds that

$$\det(\mathbf{G} - \mathbf{A}^{an}) = \frac{v(R)\cos\psi(R)}{c(R)}, \tag{C-9}$$

where the quantities $c(R)$, $v(R)$, and $\psi(R)$ denote, respectively, the phase velocity, group velocity, and angle of incidence of the group velocity vector (group angle) of the ray at the receiver. For a normal-incidence ray the points S and R are identical, and the two-way relative geometric spreading is given by the expression

$$\begin{aligned} \mathcal{L}(R, S) &= |\det \mathbf{Q}_2(R, S)|^{1/2} \\ &= \frac{v(R)}{c(R)} \cos\psi(R)\, |\det \mathbf{B}(R, S)|^{1/2}\,. \end{aligned} \tag{C-10}$$

APPENDIX D

RELATIONS BETWEEN REFLECTED WAVES, NIP WAVES, AND NORMAL WAVES

We derive the matrix relations in equations 41–42 from equation 36 for the two-way ray-propagator matrix, i.e.,

$$\mathbf{\Pi}(R, S) = \begin{bmatrix} \big(2\mathbf{Q}_{\mathrm{NIP}}\mathbf{P}_N^T + \mathbf{I}\big)\mathbf{I}^* & 2\mathbf{Q}_{\mathrm{NIP}}\mathbf{Q}_N^T\mathbf{I}^* \\ 2\mathbf{P}_{\mathrm{NIP}}\mathbf{P}_N^T\mathbf{I}^* & \big(2\mathbf{P}_{\mathrm{NIP}}\mathbf{Q}_N^T - \mathbf{I}\big)\mathbf{I}^* \end{bmatrix}. \tag{D-1}$$

Consider the following invariant from equation 37:

$$\mathbf{P}_{\mathrm{NIP}}\mathbf{Q}_N^T - \mathbf{P}_N\mathbf{Q}_{\mathrm{NIP}}^T = \mathbf{I}, \tag{D-2}$$

in which we insert $\mathbf{P}_{\mathrm{NIP}} = \mathbf{M}_{\mathrm{NIP}}\mathbf{Q}_{\mathrm{NIP}}$ and $\mathbf{P}_N = \mathbf{M}_N\mathbf{Q}_N$. The matrix $\mathbf{M}_N$ contains the second derivatives of one-way time corresponding to initialization as a normal wave at the normal-incidence point. By noting that the matrix product $\mathbf{Q}_{\mathrm{NIP}}\mathbf{Q}_N^T$ is symmetric, we get

$$\mathbf{Q}_{\mathrm{NIP}}\mathbf{Q}_N^T = (\mathbf{M}_{\mathrm{NIP}} - \mathbf{M}_N)^{-1}, \tag{D-3}$$

$$\mathbf{Q}_2(R, S) = 2(\mathbf{M}_{\mathrm{NIP}} - \mathbf{M}_N)^{-1}\mathbf{I}^*. \tag{D-4}$$

From the two-way ray-propagator matrix in equation D-1, we find that $\mathbf{P}_2(R, S) = (2\mathbf{P}_{\mathrm{NIP}}\mathbf{Q}_N^T - \mathbf{I})\mathbf{I}^* = (2\mathbf{M}_{\mathrm{NIP}}\mathbf{Q}_{\mathrm{NIP}}\mathbf{Q}_N^T - \mathbf{I})\mathbf{I}^*$, which gives

$$\mathbf{P}_2(R, S) = [2\mathbf{M}_{\mathrm{NIP}}(\mathbf{M}_{\mathrm{NIP}} - \mathbf{M}_N)^{-1} - \mathbf{I}]\mathbf{I}^*. \tag{D-5}$$

The matrix $\mathbf{M}_2(R, S)$ containing the second derivatives of two-way time corresponding to an initial point source is given by

$$\mathbf{M}_2(R, S) = \mathbf{P}_2(R, S)\mathbf{Q}_2(R, S)^{-1}. \tag{D-6}$$

Inserting equations D-4 and D-5 in equation D-6 leads to the result

$$\mathbf{M}_2(R, S) = \tfrac{1}{2}(\mathbf{M}_{\mathrm{NIP}} + \mathbf{M}_N). \tag{D-7}$$

APPENDIX E

SECOND-ORDER APPROXIMATION TO TRAVELTIMES IN THE CMP DOMAIN

This appendix reviews the derivation of a second-order approximation to traveltimes in the CMP domain, based on second-order approximations to paraxial traveltimes derived by Červený et al. (1984) and Bortfeld (1989). In the latter formulation, the general expression for the paraxial traveltime is

$$\begin{aligned} T(R', S') = T(R, S) &+ \bar{\mathbf{p}}^{(z)}(R)^T\bar{\mathbf{z}}(R') - \bar{\mathbf{p}}^{(z)}(S)^T\bar{\mathbf{z}}(S') \\ &+ \tfrac{1}{2}\bar{\mathbf{z}}(R')^T\mathbf{D}(R, S)\mathbf{B}^{-1}(R, S)\bar{\mathbf{z}}(R') \\ &+ \tfrac{1}{2}\bar{\mathbf{z}}(S')^T\mathbf{B}^{-1}(R, S)\mathbf{A}(R, S)\bar{\mathbf{z}}(S') \\ &- \bar{\mathbf{z}}(R')^T\mathbf{B}^{-1}(R, S)\bar{\mathbf{z}}(S'). \end{aligned} \tag{E-1}$$

The quantities in equation E-1 having S and/or R as arguments all correspond to a (central) ray between points S and R. The notation S' and R' is used for two points on a neighboring ray (paraxial ray). Points S' and S are located close to each other, and so are points R' and R. The two-component vectors $\bar{\mathbf{z}}(S')$ and $\bar{\mathbf{p}}^{(z)}(S')$ specify, respectively, the projections of the paraxial-position vector and slowness vector into the z_1-z_2-plane of the local-interface system at the source point S. The vectors $\bar{\mathbf{z}}(R')$ and $\bar{\mathbf{p}}^{(z)}(R')$ denote the corresponding projections of the paraxial position vector and slowness vector at receiver-point R. Points S and R correspond to zero offset and are therefore identical, and the coordinate axes of the local interface systems at S and R are both parallel to those of the model coordinate system. Thus, we have

$$\begin{aligned} \bar{\mathbf{z}}(S') &= \Delta\bar{\mathbf{x}}(S') = \bar{\mathbf{x}}(S') - \bar{\mathbf{x}}(S), \\ \bar{\mathbf{z}}(R') &= \Delta\bar{\mathbf{x}}(R') = \bar{\mathbf{x}}(R') - \bar{\mathbf{x}}(R). \end{aligned} \tag{E-2}$$

The midpoint between points S' and R' is denoted as X'. We can then apply the linear transformations from source/receiver to midpoint/half-offset coordinates (Ursin, 1982):

$$\bar{\mathbf{x}}(X') = \tfrac{1}{2}[\bar{\mathbf{x}}(S') + \bar{\mathbf{x}}(R')], \qquad \bar{\mathbf{y}} = \tfrac{1}{2}[\bar{\mathbf{x}}(S') - \bar{\mathbf{x}}(R')]. \tag{E-3}$$

The CMP domain of the seismic data is characterized by the fact that

$$\Delta\bar{\mathbf{x}}(X') = \mathbf{0}, \qquad \bar{\mathbf{y}} = \Delta\bar{\mathbf{x}}(S') = -\Delta\bar{\mathbf{x}}(R'). \tag{E-4}$$

This yields

$$\begin{aligned} T_{\mathrm{CMP}}(\bar{\mathbf{y}}) = T_0 &+ \tfrac{1}{2}\bar{\mathbf{y}}^T\mathbf{D}(R, S)\mathbf{B}^{-1}(R, S)\bar{\mathbf{y}} \\ &+ \tfrac{1}{2}\bar{\mathbf{y}}^T\mathbf{B}^{-1}(R, S)\mathbf{A}(R, S)\bar{\mathbf{y}} \\ &- \bar{\mathbf{y}}^T\mathbf{B}^{-1}(R, S)\bar{\mathbf{y}}, \end{aligned} \tag{E-5}$$

where T_0 is the two-way traveltime at zero offset. By introducing paraxial ray-tracing matrices corresponding to one-way propagation, one can alternatively write the traveltime $T_{\mathrm{CMP}}(\bar{\mathbf{y}})$ in terms of paraxial ray-tracing matrices propagated in the upward direction,

$$T_{\mathrm{CMP}}(\bar{\mathbf{y}}) = T_0 + \bar{\mathbf{y}}^T \mathbf{D}^{\uparrow} \mathbf{B}^{\uparrow -1} \bar{\mathbf{y}}, \tag{E-6}$$

or in the downward direction,

$$T_{\mathrm{CMP}}(\bar{\mathbf{y}}) = T_0 + \bar{\mathbf{y}}^T \mathbf{B}^{\downarrow -1} \mathbf{A}^{\downarrow} \bar{\mathbf{y}}. \tag{E-7}$$

We can conclude that the second derivatives of the traveltime in the CMP domain, evaluated for zero offset ($\bar{\mathbf{y}} = \mathbf{0}$), are given by

$$\frac{\partial^2 T_{\mathrm{CMP}}}{\partial y_I \partial y_J} = 2[M_{\mathrm{NIP}}]_{IJ}^{(x)}. \tag{E-8}$$

Equation E-8, derived by Chernyak and Gritsenko (1979); is referred to as the NIP-wave theorem. The quantity $[M_{\mathrm{NIP}}]_{IJ}^{(x)}$ denotes the elements of the 2×2 matrix

$$\mathbf{M}_{\mathrm{NIP}}^{(x)} = \mathbf{D}^{\uparrow} \mathbf{B}^{\uparrow -1} = \mathbf{B}^{\downarrow -1} \mathbf{A}^{\downarrow}, \tag{E-9}$$

containing the second-order derivatives of the traveltime of the NIP wave, taken with respect to the coordinates x_1, x_2 of the model coordinate system. Thus, propagation of a single hypothetical wavefront from the normal-incidence point M, i.e., the wavefront of the NIP wave, is sufficient to determine a second-order approximation to a traveltime function within the CMP domain.

REFERENCES

Bakker, P. M., 1998, Phase shift at caustics along rays in anisotropic media: Geophysical Journal International, **134**, 515–518.

———, 2002, Coupled anisotropic shear-wave ray tracing in situations when associated slowness sheets are almost tangent: Pure and Applied Geophysics, **159**, 1403–1417.

Bortfeld, R., 1989, Geometrical ray theory: Rays and traveltimes in seismic systems (second-order approximation of the traveltimes): Geophysics, **54**, 342–349.

Bulant, P., and L. Klimeš, 2002, Numerical algorithm of the coupling ray theory in weakly anisotropic media: Pure and Applied Geophysics, **159**, 1419–1435.

Červený, V., 1985, The application of ray tracing to numerical modeling of seismic wavefields in complex structures, *in* G. Dohr, ed., Seismic shear waves, part A: Theory: Geophysical Press, 1–124.

———, 2001, Seismic ray theory: Cambridge University Press.

Červený, V., L. Klimeš, and I. Pšenčík, 1984, Paraxial ray approximations in the computation of seismic wavefields in inhomogeneous media: Geophysical Journal of the Royal Astronomical Society, **79**, 89–104.

Chapman, C. H., 1994, Reflection/transmission coefficient reciprocities in anisotropic media: Geophysical Journal International, **116**, 498–501.

Chernyak, V. S., and S. A. Gritsenko, 1979, Interpretation of the effective common-depth-point parameters for a three-dimensional system of homogeneous layers with curvelinear boundaries: Soviet Geology and Geophysics, **20**, 91–98.

Coates, R. T., and C. H. Chapman, 1990, Quasi-shear wave coupling in weakly anisotropic 3-D media: Geophysical Journal International, **103**, 301–320.

Gjøystdal, H., J. E. Reinhardsen, and B. Ursin, 1984, Traveltime and wavefront curvature calculations in three-dimensional inhomogeneous layered media with curved interfaces: Geophysics, **49**, 1466–1494.

Goldin, S. V., 1991, Decomposition of geometrical spreading approximation of a reflected wave: Soviet Geology and Geophysics, **32**, 110–119.

Goldin, S. V., and V. N. Piankov, 1992, On geometrical spreading and the number of singularities on a ray: Geology and Geophysics, **33**, 90–105.

Hubral, P., 1983, Computing true amplitude reflections in a laterally inhomogeneous earth: Geophysics, **48**, 1051–1062.

Hubral, P., and T. Krey, 1980, Interval velocities from seismic reflection time measurements: SEG.

Hubral, P., J. Schleicher, and M. Tygel, 1992a, Three-dimensional paraxial ray properties: — I. Basic relations: Journal of Seismic Exploration, **1**, 265–279.

——— 1992b, Three-dimensional paraxial ray properties: — II. Applications: Journal of Seismic Exploration, **1**, 347–362.

———, 1993, Three-dimensional primary zero-offset reflections: Geophysics, **58**, 692–702.

Iversen, E., and H. Gjøystdal, 1984, Three-dimensional velocity inversion by use of kinematic and dynamic ray tracing: 54th Annual International Meeting, SEG, Expanded Abstracts, 64–645.

Klimeš, L., 1997, Phase shift of the Green function due to caustics in anisotropic media: 67th Annual International Meeting, SEG, Expanded Abstracts, 1834–1837.

Kravtsov, Y. A., and Y. I. Orlov, 1980, Geometrical optics of inhomogeneous media (in Russian): Nauka Publishing.

Popov, M. M., and I. Pšenčík, 1978, Computation of ray amplitudes in inhomogeneous media with curved interfaces: Studia Geophysica et Geodaetica, **22**, 248–258.

Pšenčík, I., 1998, Green's functions for inhomogeneous weakly anisotropic media: Geophysical Journal International, **135**, 279–288.

Pšenčík, I., and J. A. Dellinger, 2001, Quasi-shear waves in inhomogeneous weakly anisotropic media by the quasi-isotropic approach: A model study: Geophysics, **66**, 308–319.

Schleicher, J., M. Tygel, and P. Hubral, 1993a, 3-D true-amplitude finite-offset migration: Geophysics, **58**, 1112–1126.

———, 1993b, Parabolic and hyperbolic paraxial two-point traveltimes in 3D media: Geophysical Prospecting, **41**, 495–513.

Schleicher, J., M. Tygel, B. Ursin, and N. Bleistein, 2001, The Kirchhoff-Helmholtz integral for anisotropic elastic media: Wave Motion, **34**, 353–364.

Tsvankin, I., and L. Thomsen, 1994, Nonhyperbolic reflection moveout in anisotropic media: Geophysics, **59**, 1290–1304.

Ursin, B., 1982, Quadratic wavefront and travel time approximations in inhomogeneous layered media with curved interfaces: Geophysics, **47**, 1012–1021.

———, 1990, Offset-dependent geometrical spreading in a layered medium (short note): Geophysics, **55**, 492–496.

Ziolkowski, R. W., and G. A. Deschamps, 1980, The Mastov method and the asymptotic Fourier transform: Caustic analysis: University of Illinois Electromagnetic Laboratory Scientific Report 80–9.